Published by :
http://www.ijert.org

International Journal of Engineering Research & Technology (IJERT)
ISSN: 2278-0181
Vol. 10 Issue 03, March-2021

# Effective and Median Effective Earth Radius Factor Distribution Characterization for Microwave Link Design Applications

A. M. Nyete
Department of Electrical and Information Engineering
University of Nairobi

***Abstract*:- In this paper, radiosonde data is processed to obtain the point median and effective values of the effective earth radius factor (k-factor). These point values are the interpolated to obtain the effective earth distribution for the entire country by producing the contour maps from the values obtained. The accuracy of the results obtained is validated using the RMSE and MAE. The error results show that the interpolation methods used have a high degree of accuracy in predicting the k-factor values of the entire country.**

## 1. INTRODUCTION

The refractive properties of the lower atmosphere is defined in terms of the vertical profile of the radio refractivity, given by [1-6]**:**

$$N = \frac{77.6}{T}P + 3.3 \times 10^5 \frac{e}{T^2} \qquad (1)$$

where $P$ is the atmospheric pressure (hPa), $e$ is the water vapour pressure (hPa), and $T$ is the absolute temperature (K). The above Equation is valid when the radio frequency is below 100GHz with errors of less than 0.5% [5,6]. From the equation above, the radio refractivity has wet and dry components, given by [6-10]:

$$N_{dry} = \frac{77.6}{T}P \qquad (2)$$

and,

$$N_{wet} = 3.3 \times 10^5 \frac{e}{T^2} \qquad (3)$$

The vertical refractivity gradient is then given by [9-15]:

$$\frac{dN}{dh} = 77.6\left(\frac{1}{T}\frac{dP}{dh} + \frac{4810de}{T^2 dh}\right) \qquad (4)$$

In Equation (4) above, it is assumed that the radio refractivity does not vary horizontally, that is, it only varies vertically.

Due to the radio refractivity, electromagnetic waves travelling through the atmosphere suffer a degree of bending. For easier of geometrical analysis, the electromagnetic waves are normally represented as straight lines then compensation is done by assuming an imaginary earth radius, otherwise referred to as effective earth radius, $r_e$ [3]. The ratio between the effective and true earth radius is referred to as the effective earth radius factor (k-factor) and is given by [3]:

$$k = \frac{r_e}{r_o} = 1 + r_o \frac{dn}{dh} \qquad (5)$$

where $k$ is the effective earth radius factor and $r_e$ is the effective earth radius and $r_o$ is the true earth radius. The effective earth radius factor ( k-factor) is a function of the vertical refractivity gradient and can also be determined by the equation [1-3]:

$$k = \left[1 + \frac{dN/dh}{157}\right]^{-1} \qquad (6)$$

Due to the tedious work of collecting and processing radiosonde data to obtain the radio refractivity and ultimately the k-factor statistics for different location, interpolation techniques will be applied on sample data for chosen locations in South Africa to generate the contour maps necessary for link design in the whole country.

## 2. INTERPOLATION TECHNIQUES

Interpolation refers to the process of predicting data values at locations where samples are not available using data from surrounding locations within a particular geographical range (area) [14, 15]. There are two broad categories of interpolation techniques namely: global and local methods. Global methods consider all known samples to estimate the value at a given location. Local methods consider only a fixed number of samples within a certain search radius to the point being estimated. Global methods are known to produce smooth estimates but are very sensitive to outliers. On the other hand, local methods produce less smooth surfaces but are less sensitive to outliers. Global methods include trend surfaces, Fourier series and many others while local methods include Radial Basis Functions, Kriging and Inverse Distance Weighting (IDW) [14, 16], among others. The most commonly used interpolation techniques are spatial and they include: Radial Basis Functions (RBFs), Kriging and Inverse Distance Weighting (IDW). Spatial interpolation techniques are based on the proposition that things which are closer to each other are more alike than those further apart.

International Journal of Engineering Research & Technology (IJERT)
ISSN: 2278-0181
Vol. 10 Issue 03, March-2021

Due to the tedious nature of processing clear-air meteorological data, and the cost involved in launching radiosondes, the three spatial interpolation techniques listed above have been employed here in extending both the median and effective k-factor statistics obtained in Chapter 4 to cover the whole of South Africa. A comparison of the interpolation methods is drawn by using the Mean Absolute Error (MAE) and Root Mean Square Error (RMSE) criteria and then the interpolated and gridded values are presented in contour maps. The RMSE is sensitive to outliers while the MAE is not; hence both errors complement each other. Both error criteria provide an excellent averaged summary of the variation between measured and predicted values.

**2.1 Inverse Distance Weighting (IDW)**

IDW is a deterministic interpolation technique. In this method, data values that are closer to each other are assumed to be more similar than those farther apart. IDW uses a weighting scheme to evaluate the impact individual data points have on the predicted value with data points that are closer to the prediction point being assigned more weight, hence having more impact on the predicted value than those farther from the predicted value . The weighting policy in IDW is based only on the Euclidian distance between the known data points and the prediction point. The predicted estimate is then a linear combination of the weighted measured values. The weight assignment in IDW is controlled by a power parameter, $p$ that determines how much influence data points have on the predicted value as the Euclidian distance varies. The higher the power parameter, the more the influence closer points have on the predicted value and vice versa. Typically, the power parameter is assigned value of 2 or 3 but the choice can also be made based on error measurement resulting in optimal IDW. Mathematically, the IDW predictor is given by [14]:

$$k(x,y) = \sum_{i=1}^{N} w_i k(x_i, y_i) \tag{7}$$

where $k(x,y)$ is the IDW predictor, $N$ is the number of known data points, $k(x_i, y_i)$ is the known data value at the point $(x_i, y_i)$ and $w_i$ is the weight assigned to $k(x_i, y_i)$. The weight $w_i$, is given by [14]:

$$w_i = \frac{d_i^{-p}}{\sum_{i=1}^{N} d_i^{-p}} \tag{8}$$

where $p$ is the power parameter, $d$ is the Euclidian distance between the prediction point and the known data point and is given by:

$$d = \sqrt{(x - x_i)^2 + (y - y_i)^2} \tag{9}$$

where all parameters are as described in (7) and (8). The weighting in IDW is such that the sum of all the weights sum to unity:

$$\sum_{i=1}^{N} w_i = 1 \tag{10}$$

Since IDW uses a simple weighting scheme that is only based on the Euclidian distance between the known data point and the prediction point alone, the level of computational subjectivity is low hence computation speeds are faster compared to other sophisticated methods like kriging.

***2.2 Kriging***

Kriging is a stochastic interpolator but similar to IDW in that it also employs weighting to predict unknown values. Just as in IDW, the predicted value is a linear combination of the known weighted samples [14, 15]. Points closer to the prediction point are also assigned more weight compared to those farther apart. However, the weighting used in kriging is more complex and involves spatial correlation between the predicted point and known data points. This spatial correlation and interdependence in kriging is modeled using the semivariogram. The semivariogram is a plot of the semivariances against the separation distances (lag distances) of the known data points. The mathematical relationship that best describes the semivariogram is then used to build covariance matrices necessary for the determination of the kriging weights. The semivariance is a measure of the dissimilarity of a measured variable and is given by the average squared difference between the data values and is given by [14, 17]:

$$\gamma(h) = \frac{1}{2N(h)} \sum_{(i,j|h_{ij}=h)} \left(k_i - k_j\right)^2 \tag{11}$$

where $N(h)$ is the number of data values separated by a distance $h$.There are several empirical sevariogram models that can be used to model the semivariance. They include; spherical semivariogram, exponential semivariogram, cubic semivariogram, Bessel semivariogram, j-Bessel semivariogram and Gaussian semivariogram, among others [14, 16].

The semivariogram is characterized by three main coefficients namely; the range, the sill and the nugget. The range is defined as the maximum lag distance between two points for which the semivariance between them can be determined. This is to say that, if the lag distance between two data values is greater than the range, then the points are not spatially correlated or interdependent. The sill is the value of the semivariance between two data values at the lag distance equal to the range. Ideally, when the lag distance is zero, the semivariance is supposed to be zero also. This is not always the case and at times a non-zero value of the semivariance is obtained when the lag distance is zero, and this value of the semivariance is what is referred to as the nugget effect, or simply the nugget. The nugget is usually an indicator of the interpolation error and can also be attributed to spatial sources of variation at distances smaller than the sampling interval. There are different kriging techniques, namely: ordinary kriging, simple kriging, cokriging, kriging

International Journal of Engineering Research & Technology (IJERT)
ISSN: 2278-0181
Vol. 10 Issue 03, March-2021

with trend and universal kriging [15]. Of these, ordinary kriging is the one used in the current study and is the only one discussed further.

### *2.2.1 Ordinary Kriging*

In ordinary kriging, the mean is assumed constant and unknown in the local neighbourhood of the prediction point. The kriging weights sum to unity and are computed from [14, 17, 18]:

$$w_{ok} = Z_{ok}^{-1} M_{ok} \tag{12}$$

where $\lambda_{ok}$ is the kriging weights vector matrix, $Z_{ok}^{-1}$ is the covariance matrix for the known data points and $M_{ok}$ is the covariance vector matrix between the prediction data point and known data points. The kriging predictor is then given by [14, 18, 19]**:**

$$k_{ok}^{*}(x,y) = \sum_{i=1}^{N} w_{oki} k_{oki}(x_i, y_i) \tag{13}$$

where $k_{oki}(x_i, y_i)$ is the data value at point $(x_i, y_i)$, $\lambda_{oki}$ is the weight associated with it and $N$ is as defined in (7). Normally, the weights are determined by minimizing the variance of the interpolation error, otherwise referred to as the estimation error variance, $\sigma_E^2$. This is usually achieved by the introduction of a function $L$ which contains the Lagrange parameter, $\lambda$ given by [15]:

$$L = \sigma_E^2 + 2\lambda[1 - \textstyle\sum_{i=1}^{N} w_{oki}] \tag{14}$$

The minimization of the estimation error variance is then done by taking the derivative of the above function and then equating it to zero, that is, [15]:

$$\frac{1}{2}\frac{\partial L}{\partial \lambda} = 1 - \textstyle\sum_{i=1}^{N} w_{oki} = 0 \tag{15}$$

Then, the ordinary kriging weights are computed from the following matrix equation [19]:

$$\begin{bmatrix} Z(1,1) & Z(1,2) \cdots Z(1,n) & 1 \\ Z(2,1) & Z(2,2) \cdots Z(2,n) & 1 \\ \vdots & \vdots \quad \vdots & \vdots \\ Z(n,1) & Z(n,2) \cdots Z(n,n) & 1 \\ 1 & 1 \quad \ldots \quad 1 & 0 \end{bmatrix} \begin{bmatrix} w_{ok1} \\ w_{ok2} \\ \vdots \\ w_{okn} \\ \lambda \end{bmatrix} = \begin{bmatrix} M(0,1) \\ M(0,2) \\ \vdots \\ M(0,n) \\ 1 \end{bmatrix} \tag{16}$$

where $Z$(i,j) is the covariance between measured locations $i$ and $j$, $M(0,j)$ is the covariance between the prediction location 0 and measured location $j$, and $w_{oki}$ is the simple kriging weight for measured location $i$. The four different kriging semivariogram models shown in Table 1 are used in the interpolation of the k-factor for South Africa in this study. In Table 1, $c$ is the nugget, $S$ is the sill and $h$ is the value of the lag distance divided by the range.

### *2.3 Radial Basis Functions (RBFs)*

RBFs are real-valued, continuous univariate functions that are radialized by composition with the Euclidian distance as the norm, $R^d$ [20]. Radial basis functions can be thought of as fitting rubber-sheeted surface through measured data values using a mathematical function [21]. Radial basis functions (RBFs) are an efficient way of making predictions when one encounters scattered data problems [22]. Scattered data may not be of much use since one will be interested in knowing or estimating the values where data is not available, for continuity purposes. Interpolation and 1-D derivative approximations are well performed using RBFs especially where the data does not form a regular grid [23]. In [23], Carr, Fright and Beatson emphasize that RBFs do not impose any restrictions on the geometry of the measured data and therefore are very well suited for scattered data. RBFs are also known to produce sufficiently accurate interpolated values from relatively few data points and are able to retain small features of the data geometry as well as spatial distribution. Also, in [24], Franke reports that multiquadrics and thin plate splines produced the best outcome for the interpolation of scattered data. RBFs can interpolate values that fall outside the range of the measured data values. They are also known to be very sensitive to outliers. The most basic form of the RBF interpolant is given by [25]:

$$s(x) = \textstyle\sum_{k=1}^{n} \lambda_k \phi(\|x - x_k\|) \tag{17}$$

where $\|x - x_k\|$ denotes the Euclidian distance, $r$, and $\phi(r)$ is some RBF, $n$ is the number of RBFs and $\lambda_k$ is the real-valued weighting coefficient associated with each RBF.

Table 1: Semivariogram models used [14, 18]

| Model | Model Equation |
|---|---|
| Cubic | $\gamma(h) = \begin{cases} c + S \cdot (7h^2 - 8.75h^3 + 3.75h^5 - 0.75h^7) & h \le 1 \\ c + S & h \ge 1 \end{cases}$ |
| Gaussian | $\gamma(h) = c + S \cdot (1 - exp(h^2))$ |
| Exponent | $\gamma(h) = c + S \cdot (1 - exp(-3h))$ |
| Spherical | $\gamma(h) = \begin{cases} c + S \cdot \left(\frac{3}{2}h - \frac{1}{2}h^3\right) & h \le 1 \\ c + S & h \ge 1 \end{cases}$ |

Thus, RBF methods employ a linear combination of translates for one function $\phi(r)$ of a single variable. In some cases, it is pertinent to add a polynomial of first degree, $P(x)$, that describes the constant as well as the linear portions of RBF interpolant in Equation (17), and in turn maintains positive-definiteness and stability of the solution; resulting in the following new expression for the RBF interpolant [26]:

$$S(x) = \textstyle\sum_{k=1}^{n} \lambda_k \phi(\|x - x_k\|) + P(x) \tag{18}$$

Radial basis functions fall in two main categories: the piece-wise smooth and the infinitely smooth. Piece-wise smooth RBFs include powers (linear, cubic and quantic among others) and thin plate splines (TPS). The power RBFs are given by [27]:

$$\phi\,(r) = r^{2n-1}, n = 1,2,3, \ldots \ldots \ldots (19)$$

The TPS is defined by [20, 25]:

$$\phi(r) = r^2 lnr \tag{20}$$

International Journal of Engineering Research & Technology (IJERT)
ISSN: 2278-0181
Vol. 10 Issue 03, March-2021

Infinitely smooth RBFs include inverse multiquadrics (IQ), multiquadric (MQ) and the Gaussian (GA) and are defined by the following expressions respectively [25, 28]:

$$\phi(r) = \frac{1}{\sqrt{1+(\varepsilon r)^2}} \quad (21)$$

$$\phi(r) = \sqrt{1+(\varepsilon r)^2} \quad (22)$$

$$\phi(r) = e^{-(\varepsilon r)^2} \quad (23)$$

where $\varepsilon$ is the shape parameter.

The TPS and the MQ are the ones used for the interpolation of the k-factor for South Africa and are discussed briefly next. TPSs are inspired by the concept of bending an infinitely thin metal plate. They belong to a class of RBFs commonly referred to as polyharmonic or simply surface splines. Polyharmonic RBFs do not contain a shape parameter. Thin plate splines mathematically realize the idea that, when a metal plate is fixed at certain heights vertical to the plane, it tends towards a form of minimal energy, which is the form of minimal curvature [29]. They are more attractive method since they provide $C'$ continuity and minimize the energy function below [23]:

$$E(s) = \int_{R^2}' \frac{\partial^2 s}{\partial x^2} + 2\left(\frac{\partial^2 s}{\partial x \partial y}\right)^2 + \left(\frac{\partial^2 s}{\partial y^2}\right)^2 dx\, dy \quad (24)$$

over all interpolants for which the energy functional is well defined. Thus in this particular sense, the TPS is the smoothest RBF interpolant.

The function $f$, which minimizes the following factor, below, (25), is an example of an exact RBF technique and is specifically referred to as the exact spline method [30, 31]:

$$A(f) + \sum_{i=1}^{n} w_i^2 [f(x_i) - y(x_i)]^2 \quad (25)$$

where $y(x_i) = z(x_i) + \varepsilon(x_i)$ is the source of random error, $z$ is the measured value at point $x_i$ and $\varepsilon$ is the random error associated with it. The term $A(f)$ represents the smoothness of the function $f$ and the second term represents the proximity to the measured values. The smoothing function $A(f)$ determines the level of smoothness with respect to the accuracy of the interpolation. When the function is taken to zero, one performs interpolation but without any smoothing. Alternatively, pushing the value of the function to infinity results in least square fit of the data. Thus, it is important that one maintains a good smoothing trade-off for optimal interpolation. One of the best ways to achieve this is by performing generalized cross validation [17], and this is the approach adopted for this study. Cross validation statistics are the ones used for the error computations. Cross validation involves the removal of one data point at a time and then interpolating its value. This is done in turns for all data points and then the overall error statistics are calculated.

The MQ, on the other hand, is popular for many applications and has some good approximation and interpolation properties. It represents a class of RBFs that are global in nature, containing a shape parameter and are infinitely differentiable [28, 31]. The MQ can also be optimized by performing cross validation and this is the technique used here.

The RMSE and MAE are used to compare the performance of the different interpolation methods used. These errors are given by [18, 31]:

$$RMSE = \sqrt{\left(\frac{1}{N}\sum_{i=1}^{N}(k^* - k)^2\right)} \quad (26)$$

$$MAE = \frac{1}{N}\sum_{i=1}^{N}|k^* - k| \quad (27)$$

where $k^*$ is the measured value and $k$ is the cross value.

## 3. MATERIALS AND METHODS

The computed median and effective values of the k-factor values shown in Tables 2 and 3 below. These values are then interpolated to cover the rest of South Africa using the interpolation techniques discussed above, that is, kringing, inverse distance weighting and radial basis function. The seasonal and annual median and effective k-factor values are entered into a grid together with the location's coordinates; the longitude and the latitude. For the case of kriging interpolation, the semivariogram model is then chosen. For RBF, the particular choice of the RBF is done. Else the method chosen is the IDW. The values are then interpolated to cover the rest of the country between the coordinates; latitude ($15^o$ S, $35^o$ S) and longitude ($22^o$ E, $35.2^o$ E). Cross validation of the interpolation statistics is then performed and then the associated RMSE and MAE errors computed. This process is repeated for the four semivariogram models in Table 1, the TPS and MQ RBFs, and for IDW where the minimum error criteria are used as the optimal value power parameter. The interpolated values for the method that produces the least error (best interpolation method) are then copied and saved in either Microsoft Excel or notepad files.
The latitude, longitude and the k-factor matrices are then exported to MATLAB. A MATLAB code is then used for the mapping of the k-factor and development of the contour maps of the seasonal and annual k-factor for South Africa.

Table 2: Annual median ($k_{50\%}$) and effective $k_{eff}$ ($k_{99.9\%}$) values of the k-factor, 200m a.g.l

| Location | Median($k_{50\%}$) | $k_{eff}$ ($k_{99.9\%}$) |
|---|---|---|
| Bloemfontein | 1.22 | 0.51 |
| Cape Town | 1.29 | 0.49 |
| Durban | 1.27 | 0.53 |
| Polokwane | 1.26 | 0.63 |
| Pretoria | 1.20 | 0.66 |
| Upington | 1.18 | 0.49 |
| Bethlehem | 1.16 | 0.73 |

International Journal of Engineering Research & Technology (IJERT)
ISSN: 2278-0181
Vol. 10 Issue 03, March-2021

Table 3: Seasonal median and effective k-factor values

| Location | season | $k_{50\%}$ | $k_{99.9\%}$ |
|---|---|---|---|
| Bloemfontein | Feb | 1.24 | 0.49 |
| | May | 1.21 | 0.53 |
| | Aug | 1.21 | 0.54 |
| | Nov | 1.22 | 0.50 |
| Cape Town | Feb | 1.26 | 0.41 |
| | May | 1.29 | 0.48 |
| | Aug | 1.3 | 0.52 |
| | Nov | 1.27 | 0.46 |
| Durban | Feb | 1.28 | 0.54 |
| | May | 1.26 | 0.58 |
| | Aug | 1.26 | 0.55 |
| | Nov | 1.26 | 0.63 |
| Polokwane | Feb | 1.27 | 0.64 |
| | May | 1.27 | 0.57 |
| | Aug | 1.23 | 0.66 |
| | Nov | 1.23 | 0.64 |
| Pretoria | Feb | 1.22 | 0.59 |
| | May | 1.19 | 0.58 |
| | Aug | 1.19 | 0.61 |
| | Nov | 1.20 | 0.62 |
| Upington | Feb | 1.14 | 0.43 |
| | May | 1.20 | 0.38 |
| | Aug | 1.19 | 0.44 |
| | Nov | 1.16 | 0.37 |
| Bethlehem | Feb | 1.16 | 0.72 |
| | May | 1.21 | 0.78 |
| | Aug | 1.17 | 0.58 |
| | Nov | 1.14 | 0.64 |

while for August the largest errors are produced by the MQ. For November, the TPS produces the largest RMSE errors while the MQ produces the largest MAE.

Thus, overall, we note that the IDW method posts the best error performance in terms of either the RMSE or the MAE or both. The error performance variations can be attributed to differences in k-factor values for both seasonal and annual cases as well as median and effective values as well. Also the errors variations are subject to the different parameters in each individual interpolation function as well as the spatial distribution of the data. It is worthy to note there is always no preferred interpolation method over another and that is why the two different measures of fit are used to determine the best method in different application scenarios. In our case, the IDW comes out as the best method (in terms of error) and is the one chosen for the mapping of the k-factor. The strong IDW error performance could be attributed to the fact that all its interpolated values fall within the range of the measured values. All the other methods used can interpolate values outside the range of the measured data. The dismal performance exhibited by the RBFs could be attributed to the fact that they do well with gently varying data and this is not the case with the values measured. Figures 1-5 show the contour maps for the annual and seasonal median k-factor. Figures 6-10 show the contour maps for the annual and seasonal effective k-factor.

## 4. INTERPOLATION RESULTS AND DISCUSSION

The interpolation errors are tabulated in Tables 4-7. Table 4 shows the seasonal median k-factor interpolation errors. From this table, we see that for the months of February, August and November, the Gaussian semivariogram model produces the worst error performance while IDW produces the least error. For the month of May, IDW produces the least RMSE error while the cubic semivariogram model produces the least MAE error. Table 5 shows the annual median k-factor interpolation errors. From this table, we see that IDW method produces the least RMSE and MAE errors while the Gaussian semivariogram model produces the largest interpolation errors. Table 6 shows the annual effective k-factor interpolation errors. From this table, IDW produces the least errors while Gaussian semivariogram model produces the largest RMSE error and TPS produces the largest MAE error. Table 7 shows the seasonal effective k-factor interpolation errors. From this table, we see that IDW performs best in terms of the two error criteria used for the months of February, May and November. For the month of August, the best RMSE performance is produced by IDW while the best MAE is produced by the Gaussian semivariogram model. Also, from the same table, the Gaussian semivariogram model posts the largest errors for the months of February and May

International Journal of Engineering Research & Technology (IJERT)
ISSN: 2278-0181
Vol. 10 Issue 03, March-2021

Table 4: Seasonal median k-factor interpolation errors

| | Errors | Kriging semivariogram models | | | | Radial Basis Functions | | Inverse Distance weighting |
|---|---|---|---|---|---|---|---|---|
| | | Spherical | Exponential | Gaussian | Cubic | TPS | MQ | |
| Feb | RMSE | 0.064 | 0.065 | 0.205 | 0.096 | 0.099 | 0.090 | 0.046 |
| | MAE | 0.059 | 0.060 | 0.174 | 0.081 | 0.091 | 0.081 | 0.037 |
| May | RMSE | 0.038 | 0.042 | 0.080 | 0.038 | 0.054 | 0.065 | 0.034 |
| | MAE | 0.030 | 0.033 | 0.055 | 0.029 | 0.038 | 0.049 | 0.031 |
| Aug | RMSE | 0.037 | 0.040 | 0.091 | 0.049 | 0.056 | 0.061 | 0.033 |
| | MAE | 0.039 | 0.036 | 0.074 | 0.043 | 0.050 | 0.051 | 0.029 |
| Nov | RMSE | 0.056 | 0.055 | 0.204 | 0.088 | 0.088 | 0.076 | 0.040 |
| | MAE | 0.051 | 0.052 | 0.177 | 0.074 | 0.078 | 0.70 | 0.032 |

Table 5: Annual median k-factor interpolation errors

| Errors | Kriging semivariogram models | | | | Radial basis functions | | Inverse distance weighting |
|---|---|---|---|---|---|---|---|
| | Cubic | Exponential | Spherical | Gaussian | TPS | MQ | |
| RMSE | 0.071 | 0.053 | 0.052 | 0.134 | 0.076 | 0.078 | 0.042 |
| MAE | 0.061 | 0.049 | 0.047 | 0.110 | 0.069 | 0.068 | 0.033 |

Table 6: Annual effective k-factor interpolation errors

| Errors | Kriging semivariogram models | | | | Radial basis functions | | Inverse distance weighting |
|---|---|---|---|---|---|---|---|
| | Cubic | Exponential | Spherical | Gaussian | TPS | MQ | |
| MAE | 0.126 | 0.086 | 0.088 | 0.023 | 0.126 | 0.112 | 0.057 |
| RMSE | 0.146 | 0.101 | 0.105 | 0.285 | 0.159 | 0.134 | 0.066 |

Table 7: Seasonal effective k-factor interpolation errors

| | Errors | Kriging semivariogram models | | | | Radial Basis Functions | | Inverse Distance weighting |
|---|---|---|---|---|---|---|---|---|
| | | Spherical | Exponential | Gaussian | Cubic | TPS | MQ | |
| Feb | RMSE | 0.106 | 0.102 | 0.402 | 0.169 | 0.176 | 0.138 | 0.067 |
| | MAE | 0.086 | 0.085 | 0.355 | 0.157 | 0.147 | 0.114 | 0.046 |
| May | RMSE | 0.134 | 0.129 | 0.447 | 0.20 | 0.218 | 0.179 | 0.080 |
| | MAE | 0.110 | 0.105 | 0.392 | 0.181 | 0.173 | 0.142 | 0.062 |
| Aug | RMSE | 0.058 | 0.063 | 0.056 | 0.052 | 0.105 | 0.107 | 0.044 |
| | MAE | 0.042 | 0.046 | 0.030 | 0.038 | 0.068 | 0.075 | 0.036 |
| Nov | RMSE | 0.060 | 0.065 | 0.094 | 0.058 | 0.106 | 0.106 | 0.048 |
| | MAE | 0.050 | 0.055 | 0.075 | 0.047 | 0.076 | 0.081 | 0.045 |

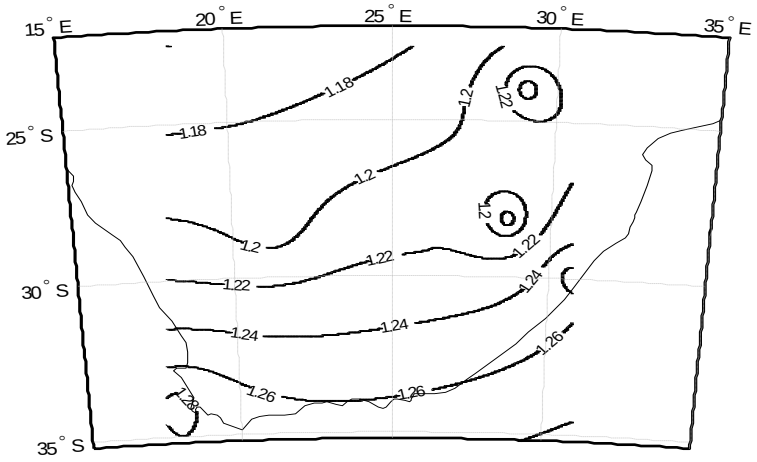


Figure 1: Three-year annual median k-factor contours for South Africa

International Journal of Engineering Research & Technology (IJERT)
ISSN: 2278-0181
Vol. 10 Issue 03, March-2021

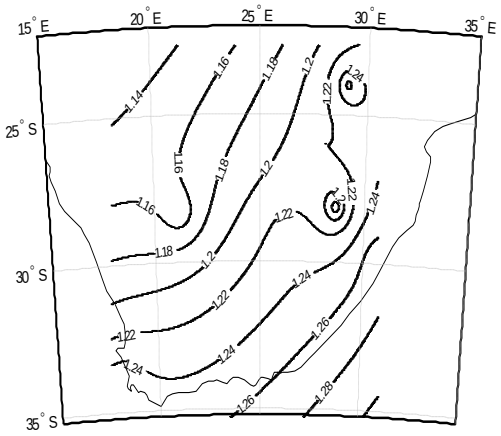


Figure 2: Three-year seasonal median k-factor contours for South Africa for the month of February

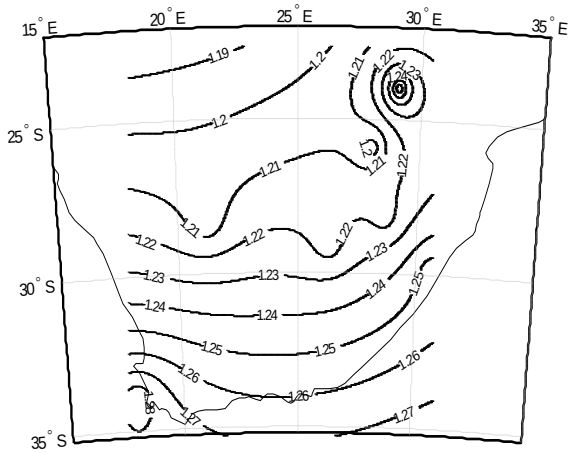


Figure 3: Three-year seasonal median k-factor contours for South Africa for the month of May

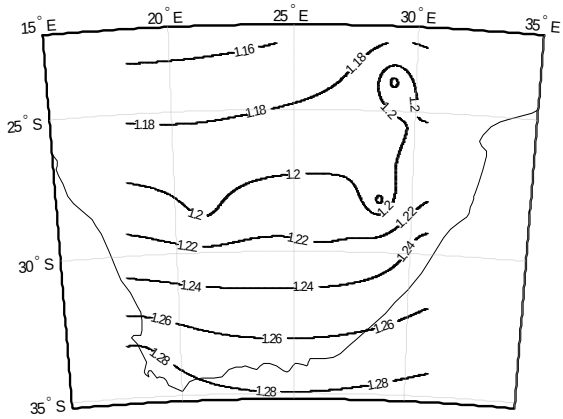


Figure 4: Three-year seasonal median k-factor contours for South Africa for the month of August

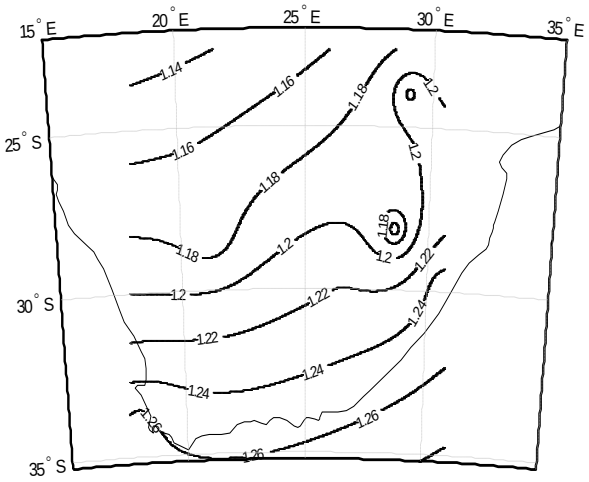


Figure 5: Three-year seasonal median k-factor contours for South Africa for the month of November

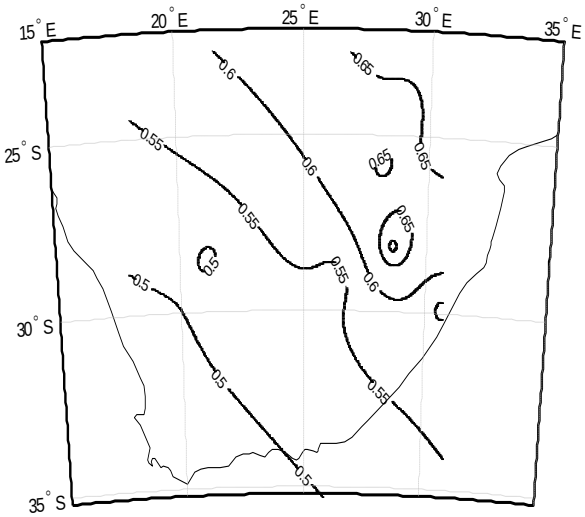


Figure 6: Three-year annual effective k-factor contours for South Africa

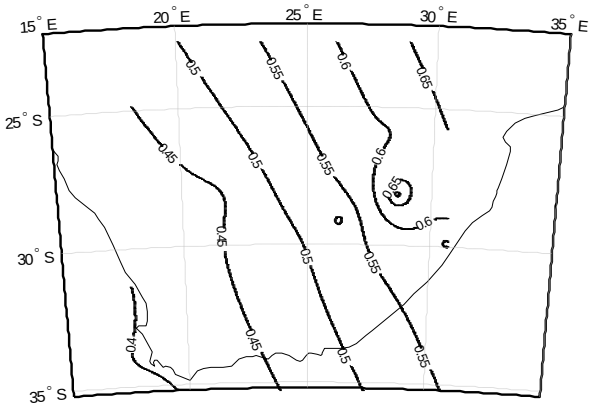


Figure 7: Three-year seasonal effective k-factor contours for South Africa for the month of February

International Journal of Engineering Research & Technology (IJERT)
ISSN: 2278-0181
Vol. 10 Issue 03, March-2021

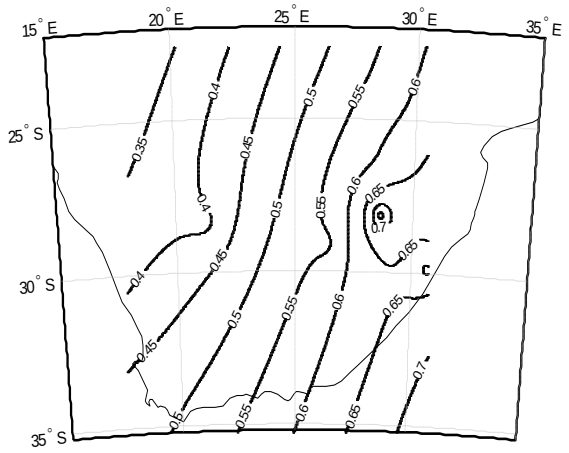


Figure 8: Three-year seasonal effective k-factor contours for South Africa for the month of May

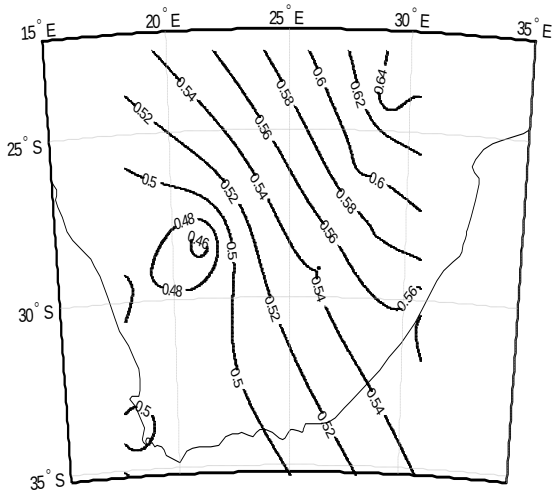


Figure 9: Three-year seasonal effective k-factor contours for South Africa for the month of August

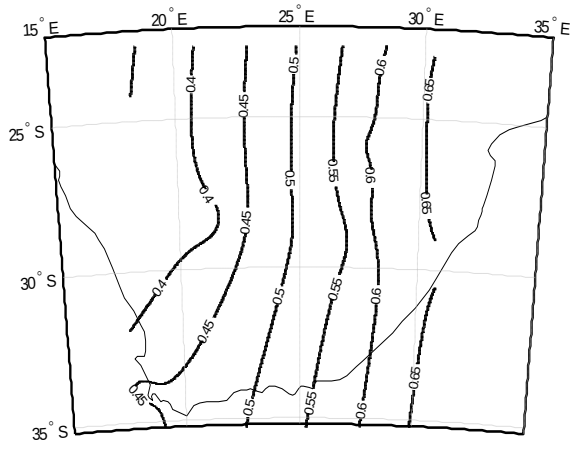


Figure 10: Three-year seasonal effective k-factor contours for South Africa for the month of November

## 5. CONCLUSION

In this paper, three spatial interpolation methods with seven different interpolation options have been considered in an effort to extend discrete k-factor values measured at seven locations in South Africa to cover the rest of the country. In order to determine which method best fits the k-factor values measured, two error criteria have been used to identify the most appropriate method. The performance of any spatial interpolation method is driven by the geometrical distribution of the data, the variation between the maximum and minimum values as well as the interpolation function used and the parameters that control the interpolation. The IDW method has been used to generate the contour maps of the k-factor for South Africa owing to its strong error performance as compared to all the other six options considered. Overall, the median k-factor contours show a decreasing trend of the k-factor as we move from the coastal regions towards the semi-arid regions in the northern and north-western parts of South Africa. Also, the effective k-factor contours show a decreasing trend of the k-factor as we move from east to west. The decreasing trend of the k-factor is consistent with the values obtained by Afullo and Odedina for Maun, Botswana [32]. This would mean that, moving further north towards Botswana, the k-factor values would diminish and a value close to the one obtained in their earlier reports would be obtained. All the interpolated values lie between the respective maximum and the values of the k-factor observed and, thus, the theory of the "edge effect" associated with IDW interpolation has been proven.

## ACKNOWLEDGENTS

The author wishes to acknowledge the South African Weather Service (SAWS) for the data used in this work.

## REFERENCES

[1] Ukhurebor K. E and Odesanya I., "Relationship between Meteorological Variables and Effective Earth Radius Factor over Auchi, Edo State, South-South, Nigeria," Covenant Journal of Physical & Life Sciences (CJPL) Vol. 7 No. 1, March, 2019 (SE).

[2] Etokebe Iniobong Jackson, Kufre M. Udofia, Ezenugu Isaac A., "Determination of Atmospheric Effective Earth Radius Factor (k-factor) Under Clear Air in Lagos, Nigeria," Mathematical and Software Engineering, Vol. 2, No. 1 (2016), 30-34.

[3] Eduediuyai Dan, Enyenihi Johnson and Idorenyin Markson, " Analysis of the effect of variations in refractivity gradient on line of sight percentage clearance and single knife edge diffraction loss," International Journal of Sustainable Energy and Environmental Research, 2019 Vol. 8, No. 1, pp. 1-9.

[4] Atijosan, A. O., Badru, R. A., Muibi, K. H., Ogunyemi, S. A., & Alaga, A. T. (2015). Effective Earth Radius Factor Prediction and Mapping for Ondo State, South Western Nigeria. Journal of Scientific Research and Reports, 6(7), 540-548. https://doi.org/10.9734/JSRR/2015/16160.

[5] Ozuomba Simeon, Kalu Constance and Ezuruike Okafor S.F., "Analysis of Variation in the Vertical Profile Of Radio Refractivity Gradient and its impact on the Effective Earth Radius Factor," International Multilingual Journal of Science and Technology (IMJST) ISSN: 2528-9810 Vol. 3 Issue 11, November 2018.

[6] Asiyo M.O and T.J Afullo, " Statistical estimation of fade depth and outage probability due to multipath propagation in South Africa,'' Progress in Electromagnetics Research B, Vol. 46, pp. 251-274, 2013.

[7] Chaudhary N.K, D.K Trivedi and R. Gupta, "The impact of k-factor on wireless link in Indian semi-desert terrain," Int.J.

International Journal of Engineering Research & Technology (IJERT)
ISSN: 2278-0181
Vol. 10 Issue 03, March-2021

Adavanced Networking and Applications, Vol. 2, No. 4 pp. 776-779, 2011.

[8] Nel J.W, S.J Erasmus and S. Mare, "The establishment of a radio refractivity database for Southern Africa", IEEE, TH0219-6/88/0000-0144, 1988.

[9] Ajayi G.O, "Physics of the Troposphere Radio-propagation," International Centre for Theoretical Physics, Internal Report No. IC/89/23, Miramare, Trieste, Italy, February 1989.

[10] Freeman R.L, Radio system design for telecommunications, Third Edition, WILEY-INTERSCIENCE: John Wiley & Sons Inc., New York, 2007.

[11] Adediji A.T, M.O Ajewole, S.E Falodun and O.R Oladosu, "Radio refractivity measurement at 150m altitude on TV tower at Akure, South-West Nigeria,'' Journal of Engineering and Applied Sciences, 2(8):1308, 2007.

[12] ITU-R, "The radio refractive index: Its formula and refractivity data," ITU-R Recommendation P.453-12.

[13] Al-Ansari K, A.A Abdulhadi and R. Kamel, "Statistical analysis of refractivity in UAE,'' International Symposium on Rainfall Rate and Radio Wave Propagation, 2007.

[14] A.M. Nyete and T.J.O Afullo, "Seasonal distribution modelling and mapping of the effective earth radius factor for microwave link design in South Africa," Progress in Electromagnetics Research B, vol. 51, 1-32, 2013.

[15] G. Bohling, Kriging, Kansas Geological Survey, C&PE 940 Report, 19th October 2005.

[16] K. Johnston, J.M. Hoef, K. Krivoruchko and N. Lucas, Using ArcGIS Geostatistical Analyst, GIS by ESRI, USA, 2001.

[17] Boer E.P.J, K.M de Beurs and A.W Hartkamp, "Kriging and thin plate splines for mapping climatic variables," JAG. vol. 3, No. 2, pp. 146-154, 2001.

[18] A.M Nyete and T.J.O Afullo, "Interpolation and mapping of the median k-factor for terrestrial link applications in South Africa," IEEE AFRICON2013 Proceedings, 9-12 September 2013, Mauritius, pp. 208-211.

[19] N. E. LeMay, Jr., "Variogram modeling and estimation," MSc. Thesis in Applied Mathematics, University of Colorado, 1995.

[20] S.A Sarra, "Integrated multiquadric radial basis function approximation methods," Computers and Mathematics with Applications 0 (2006), 1-0 Elsevier Science Ltd.

[21] S. Anderson, "An evaluation of spatial interpolation methods on air temperature in Phoenix, AZ," Tempe, AZ 85287-0104, Department of Geography, Arizona State University.

[22] J.B Cherrie, R.K Beatson and G.N Newsam, "Fast evaluation of radial basis function: Methods for generalized multiquadrics in R^n," AMS subject classifications 65D07, 41A15, 41A58, pp. 1-24.

[23] J.C Carr, W.R Fright and R.K Beatson "Surface interpolation with radial basis function for radial imaging," IEEE Transactions on Medical Imaging, vol. 16, No.1, pp.96-107, February 1997.

[24] R. Franke, "Scattered data interpolation: Tests of some method," Mathematics of Computation, vol. 38, No. 157, pp. 181-200, 1982.

[25] B. Fornberg and N. Flyer, Accuracy of radial basis function interpolation and derivative approximations on 1-D infinite grids, University of Colorado and National Center for Atmospheric Research.

[26] Morse et. al., Interpolating implicit surfaces from scattered surface data using compactly supported radial basis functions, Department of Computer Science, Brigham Young University.

[27] S.R Karur and P.A Ramachandran, "Augmented thin plate spline approximation in DRM," Boundary Element Communications, vol. 6 pp.55-58, 1995.

[28] Sarra et al., Multiquadric radial basis function approximation methods for the numerical solution of partial differential equations, Marshall University, June 2009.

[29] Lux et al., "Effects of early activator treatment in patients with class II malocclusion evaluated by thin-plate spline analysis," Angle Orthodontist, vol. 71, No.2, pp. 120-126, 2001.

[30] C.G Karydas et al., "Evaluating spatial interpolation techniques for mapping agricultural topsoil proprties in Crete," EARSeL eProceedings 8, 1/2009, pp. 26-39.

[31] A.M Nyete and T.J.O Afullo, "On the application of radial basis functions for the interpolation of the seasonal effective earth radius factor for South Africa," Southern Africa Telecommunication Networks and Applications Conference, 1-4 September 2013, Spier, Stellenbosch, Western Cape, South Africa, pp. 365-368.

[32] T.J. Afullo and P.K Odedina, "On the k-factor distribution and diffraction fading for Southern Africa," SAIEE Africa Research Journal, vol. 97(2), pp. 172-181, 2006.